

# Modelling sub-daily precipitation extremes with the blended generalised extreme value distribution

Silius M. Vandeskog<sup>1</sup>    Sara Martino<sup>1</sup>    Daniela Castro-Camilo<sup>2</sup>  
Håvard Rue<sup>3</sup>

<sup>1</sup> Norwegian University of Science and Technology (NTNU)

<sup>2</sup> University of Glasgow

<sup>3</sup> King Abdullah University of Science and Technology (KAUST)

## Abstract

A new method is proposed for modelling the yearly maxima of sub-daily precipitation, with the aim of producing spatial maps of return level estimates. Yearly precipitation maxima are modelled using a Bayesian hierarchical model with a latent Gaussian field, with the blended generalised extreme value (bGEV) distribution used as a substitute for the more standard generalised extreme value (GEV) distribution. Inference is made less wasteful with a novel two-step procedure that performs separate modelling of the scale parameter of the bGEV distribution using peaks over threshold data. Fast inference is performed using integrated nested Laplace approximations (INLA) together with the stochastic partial differential equation (SPDE) approach, both implemented in R-INLA. The model is fitted to yearly maxima of sub-daily precipitation from the south of Norway, and is able to quickly produce high-resolution return level maps with uncertainty. Using cross-validation, we find that the proposed two-step procedure provides an improved model fit when modelling sub-daily precipitation data.

**Keywords:** bGEV distribution, Block maxima modelling, INLA, Spatial statistics

## 1 Introduction

Heavy rainfall over short periods of time can cause flash floods, large economic losses and immense damage to infrastructure. The World Economic Forum states that climate action failure and extreme weather events are perceived among the most likely and most impactful global risks in 2021 (World Economic Forum, 2021). Therefore, a better understanding of heavy rainfall can be of utmost importance for many decision-makers, e.g., those that are planning the construction or maintenance of important infrastructure. In this paper, we create spatial maps with estimates of large return levels for sub-daily precipitation in Norway. Estimation of return levels is best described within the framework of extreme value theory, where the most common methods are the block maxima and the peaks over threshold (e.g. Coles, 2001; Davison & Huser, 2015). Due to low data quality (see Section 2 for more details) and the difficulty of selecting high-dimensional thresholds, we choose to use the block maxima method for estimating the precipitation return levels. This method is based on modelling the maximum of a large block of random variables with the generalised

extreme value (GEV) distribution, which is the only non-degenerate limit distribution for a standardised block maximum (Fisher & Tippett, 1928). When working with environmental data, blocks are typically chosen to have a size of one year (Coles, 2001). Inference with the GEV distribution is difficult, partially because its support depends on its parameter values. Castro-Camilo et al. (2021) propose to ease inference by substituting the GEV distribution with the blended generalised extreme value (bGEV) distribution, which has the right tail of a Fréchet distribution and the left tail of a Gumbel distribution, resulting in a heavy-tailed distribution with a parameter-free support. Vandeskog et al. (2021) demonstrate that the bGEV distribution performs well as a substitute for the GEV distribution when its tail parameter is non-negative. Consequently, we choose to use the bGEV distribution for modelling the yearly maxima of sub-daily precipitation.

Modelling of extreme daily precipitation has been given much attention in the literature, and it is well established that precipitation is a heavy-tailed phenomenon (e.g. Katz et al., 2002; Papalexiou & Koutsoyiannis, 2013; Wilson & Toumi, 2005), which makes the bGEV distribution a possible model for yearly precipitation maxima. Spatial modelling of extreme daily precipitation has also received a great amount of interest. Cooley et al. (2007) combine Bayesian hierarchical modelling with a generalised Pareto likelihood for estimating large return values for daily precipitation. Similar methods are also applied by Davison et al. (2012), Geirsson et al. (2015), Opitz et al. (2018), and Sang and Gelfand (2009), using either the block maxima or the peaks over threshold approach. Using a multivariate peaks over threshold approach, Castro-Camilo and Huser (2020) propose local likelihood inference for a specific factor copula model to deal with complex non-stationary dependence structures of precipitation over the contiguous U.S. Spatial modelling of extreme sub-daily precipitation is more difficult, due to less available data sources. Consequently, this is often performed using intensity-duration-frequency relationships where one pools together information from multiple aggregation times in order to estimate return levels (Koutsoyiannis et al., 1998; Lehmann et al., 2016; Ulrich et al., 2020; Wang & So, 2016). Spatial modelling of extreme hourly precipitation in Norway has previously been performed by Dyrørdal et al. (2015). After their work was published, the number of observational sites for hourly precipitation in Norway has greatly increased. We aim to improve their return level estimates by including all the new data that have emerged over the last years. We model sub-daily precipitation using a spatial Bayesian hierarchical model with a bGEV likelihood and a latent Gaussian field. In order to keep our model simple, we do not pool together information from multiple aggregation times, making our model purely spatial. The model assumes conditional independence between observations, which makes it able to estimate the marginal distribution of extreme sub-daily precipitation at any location, but unable to successfully estimate joint distributions over multiple locations. In the case of hydrological processes such as precipitation, ignoring dependence might lead to an underestimation of the risk of flooding. However, Davison et al. (2012) find that models where the response variables are independent given some latent process can be a good choice when the aim is to estimate a spatial map of marginal return levels.

High-resolution spatial modelling can demand a lot of computational resources and be highly time-consuming. The framework of integrated nested Laplace approximations (INLA; Rue et al., 2009) allows for a considerable speed-up by using numerical approximations instead of sampling-based inference methods like Markov chain Monte Carlo (MCMC). Inference with

a spatial Gaussian latent field can be even further sped up with the so-called stochastic partial differential equation (SPDE; Lindgren et al., 2011) approach of representing a Gaussian random field using a Gaussian Markov random field that is the approximate solution of a specific SPDE. Both INLA and the SPDE approach have been implemented in the R-INLA library, which is used for performing inference with our model (Bakka et al., 2018; Bivand et al., 2015; Rue et al., 2017).

A downside of the block maxima method is that inference can be somewhat wasteful compared to the peaks over threshold method. Additionally, most of the available weather stations in Norway that measure hourly precipitation are young and contain quite short time series. This data sparsity makes it challenging to place complex models on the parameters of the bGEV distribution in the hierarchical model. A promising method of accounting for data-sparsity is the recently developed sliding block estimator, which allows for better data utilisation by not requiring that the block maxima used for inference come from disjoint blocks (Bücher & Segers, 2018; Zou et al., 2019). However, to the best of our knowledge, no theory has yet been developed for using the disjoint block estimator on non-stationary time series, or for performing Bayesian inference with the disjoint block estimator. Vandeskog et al. (2021) propose a new two-step procedure that allows for less wasteful and more stable inference with the block maxima method by separately modelling the scale parameter of the bGEV distribution using peaks over threshold data. Having modelled the scale parameter, one can standardise the block maxima so the scale parameter can be considered as a constant, and then estimate the remaining bGEV parameters. Bücher and Zhou (2021) suggests that, when modelling stationary time series, the peaks over threshold technique is preferable over block maxima if the interest lies in estimating large quantiles in the stationary distribution of the times series. The opposite holds if the interest lies in estimating return levels, i.e. quantiles in the distribution of the block maxima. Thus, both methods have different strengths, and by using this two-step procedure, one can take advantage of the merits and improve the pitfalls of both methods. We apply the two-step procedure for modelling sub-daily precipitation and compare the performance with that of a standard block maxima model where all the bGEV parameters are estimated jointly.

The remainder of the paper is organised as follows. Section 2 introduces the hourly precipitation data and all explanatory variables used for modelling. Section 3 presents the bGEV distribution and describes the Bayesian hierarchical model along with the two-step modelling procedure. A score for evaluating model performance is also presented. In Section 4 we perform modelling of the yearly precipitation maxima in Norway. A cross-validation study is performed for evaluating the model fit, and a map of return levels is estimated. Conclusions are presented in Section 5.

## 2 Data

### 2.1 Hourly precipitation data

Observations of hourly aggregated precipitation from a total of 380 weather stations in the south of Norway are downloaded from an open archive of historical weather data from MET Norway (<https://frost.met.no>). The oldest weather stations contain observations from 1967,

but approximately 90 percent of the available weather stations are established after 2000. Each observation comes with a quality code, but almost all observations from before 2005 are of unknown quality. An inspection of the time series with unknown quality detects unrealistic precipitation observation ranging from  $-300$  mm/hour to  $400$  mm/hour. Other unrealistic patterns, like  $50$  mm/hour precipitation for more than three hours in a row, or no precipitation during more than half a year, are also detected. The data set contains large amounts of missing data, but these are often recorded as  $0$  mm/hour, instead of being recorded as missing. Thus, there is no way of knowing which of the zeros represent missing data and which represent an hour without precipitation. Having detected all of this, we decide to remove all observations with unknown or bad quality flags, which accounts for approximately 14% of the total number of observations. Additionally, we clean the data by removing all observations from years with more than 30% missing data and from years where more than two months contain less than 20% of the possible observations. This data cleaning is performed to increase the probability that our observed yearly maxima are close or equal to the true yearly maxima. Having cleaned the data, we are left with 72% of the original observations, distributed over 341 weather stations and spanning the years 2000 to 2020. The total number of usable yearly maxima is approximately 1900. Figure 1 displays the distribution of the number of usable yearly precipitation maxima per weather station. The majority of the weather stations contain five or less usable yearly maxima, and approximately 50 stations have more than 10 usable maxima. Figure 1 also displays the location of all the weather stations. A large amount of the stations are located close to each other, in the southeast of Norway. This is where the population density is at its largest. In general, there seems to be a high correlation between the density of weather stations and the population density of Norway. The correlation seems to be approximately independent of the ages of the weather stations. However, there is still a good spatial coverage of the entire area of interest, even for areas with low population densities.

The yearly maxima of precipitation accumulated over  $1, 2, \dots, 24$  hours are computed for all locations and available years. A rolling window approach with a step size of 1 hour is used for locating the precipitation maxima. As noted by Robinson and Tawn (2000), a sampling frequency of one hour is not enough to observe the exact yearly maximum of hourly precipitation. With this sampling frequency, one only observes the precipitation during the periods 00:00-01:00, 01:00-02:00, etc., whereas the maximum precipitation might occur e.g. during the period 14:23-15:23. Approximately half of the available weather stations have a sampling frequency of one minute, while the other half only contain hourly observations. We therefore use a sampling frequency of one hour for all weather stations, as this allows us to use all the 341 weather stations without having to account for varying degrees of sampling frequency bias in our model.

Dyrddal et al. (2015) used the same data source for estimating return levels of hourly precipitation. They fitted their models to hourly precipitation maxima using only 69 weather stations from all over Norway. However, they received a cleaned data set from the Norwegian Meteorological Institute, resulting in time series with lengths up to 45 years. Our data cleaning approach is more strict than that of Dyrddal et al. (2015) in the sense that it results in shorter time series by removing all data of uncertain quality. On the other hand, we include more locations and get a considerably better spatial coverage, by keeping all time series with at least one good year of observations.

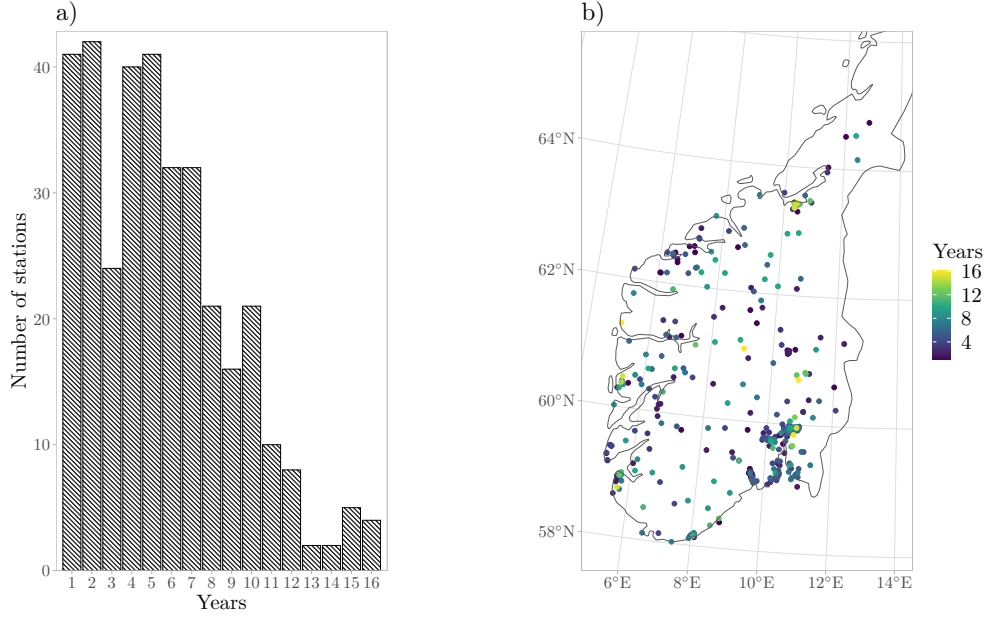


Figure 1: a) A histogram displaying the number of usable yearly precipitation maxima for all the weather stations used in this paper. b) The location of the 341 weather stations. The number of usable yearly precipitation maxima from each station are displayed using different colours. Note that some points overlap in areas with high station densities.

The main focus of this paper is the novel methodology for fast and simple estimation of return levels, and we believe that we have prepared the data well enough to give a good demonstration of our proposed model and to achieve reliable return level estimates for sub-daily precipitation. It is trivial to add more, or differently cleaned data, to improve the return level estimates at a later time.

## 2.2 Explanatory variables

We use one climate-based and four orographic explanatory variables. These are displayed in Table 1. Altitude is extracted from a digital elevation model of resolution  $50 \times 50 \text{ m}^2$ , from the Norwegian Mapping Authority (<https://hoydedata.no>). The distance to the open sea is computed using the digital elevation model. Precipitation climatologies for the period 1981-2010 are modelled by Crespi et al. (2018). The climatologies do not cover the years 2011-2020, from which most of the observations come. We assume that the precipitation patterns have not changed overly much and that they are still representative for the years 2011-2020. Hanssen-Bauer and Førland (1998) find that, in most southern regions of Norway, the only season with a significant increase in precipitation is Autumn. This strengthens our assumption that the change in precipitation patterns is slow enough to not be problematic for us.

Dyrørdal et al. (2015) include additional explanatory variables in their model, such as temperature, summer precipitation and the yearly number of wet days. They find mean

Table 1: Explanatory variables used for modelling sub-daily precipitation extremes. The two rightmost columns show which explanatory variables are used for modelling which parameters of the bGEV distribution for yearly precipitation (see Section 3.2).

Explanatory variable	Description	Unit	$\mathbf{x}_\mu$	$\mathbf{x}_\sigma$
Mean annual precipitation	Mean annual precipitation for the years 1981-2010	mm	✓	
Easting	Eastern coordinate (UTM 32)	km	✓	✓
Northing	Northern coordinate (UTM 32)	km	✓	✓
Altitude	Height above sea level	m	✓	
Distance to the open sea	Shortest distance to the open sea	km	✓	✓

summer precipitation to be one of the most important explanatory variables. We compute these explanatory variables at all station locations using the gridded seNorge2 data product (Lussana, Saloranta, et al., 2018; Lussana, Tveito, et al., 2018). Our examination finds that yearly precipitation, summer precipitation and the yearly number of wet days are close to 90% correlated with each other. There is also a negative correlation between temperature and altitude of around -85%. Consequently, we choose to not use any more explanatory variables for modelling, as highly correlated variables might lead to identifiability issues during parameter estimation.

## 3 Methods

### 3.1 The bGEV distribution

Extreme value theory concerns the statistical behaviour of extreme events, possibly larger than anything ever observed. It provides a framework where probabilities associated with these events can be estimated by extrapolating into the tail of the distribution. This can be used for e.g. estimating large quantiles, which is the aim of this work (e.g. Coles, 2001; Davison & Huser, 2015). A common approach in extreme value theory is the block maxima method. Assume that the limiting distribution of the standardised block maximum  $(Y_k - b_k)/a_k$  is non-degenerate, where  $Y_k = \max\{X_1, X_2, \dots, X_k\}$  is the maximum over  $k$  random variables from a stationary stochastic process, and  $\{b_k\}$  and  $\{a_k > 0\}$  are some appropriate sequences of standardising constants. Then, for large enough block sizes  $k$ , the distribution of the block maximum  $Y_k$  is approximately equal to the GEV distribution (Coles, 2001; Fisher & Tippett, 1928)

$$P(Y_k \leq y) \approx \begin{cases} \exp \left\{ -[1 + \xi(y - \mu_k)/\sigma_k]_+^{-1/\xi} \right\}, & \xi \neq 0, \\ \exp \left\{ -\exp[-(y - \mu_k)/\sigma_k] \right\}, & \xi = 0, \end{cases} \quad (1)$$

where  $(a)_+ = \max\{a, 0\}$ ,  $\sigma_k > 0$  and  $\mu_k, \xi \in \mathbb{R}$ . In most settings,  $k$  is fixed, so we denote  $\sigma = \sigma_k$  and  $\mu = \mu_k$ . Using the block maxima method for estimating tail probabilities has



the drawback that inference is somewhat wasteful, as only one out of every  $k$  observations are used for inference. Another challenge connected to the GEV distribution is that its support depends on its parameters. This complicates inference procedures such as maximum likelihood estimation (e.g. Bücher & Segers, 2017; Smith, 1985), and can be particularly problematic in a covariate-dependent setting with spatially varying parameters, as it might also introduce artificial boundary restrictions such as an unnaturally large lower bound for yearly maximum precipitation. Castro-Camilo et al. (2021) propose the bGEV distribution as an alternative to the GEV distribution in settings where the tail parameter  $\xi$  is non-negative. The support of the bGEV distribution is parameter-free and infinite. This allows for more numerically stable inference, while also avoiding the possibility of estimated lower bounds that are larger than future observations. The bGEV distribution function is

$$H(y; \mu, \sigma, \xi, a, b) = F(y; \mu, \sigma, \xi)^{v(y; a, b)} G(y; \tilde{\mu}, \tilde{\sigma})^{1-v(y; a, b)}, \quad (2)$$

where  $F$  is a GEV distribution with  $\xi \geq 0$  and  $G$  is a Gumbel distribution. The weight function is equal to

$$v(y; a, b) = F_\beta \left( \frac{y - a}{b - a}; c_1, c_2 \right),$$

where  $F_\beta(\cdot; c_1, c_2)$  is the distribution function of a beta distribution with parameters  $c_1 = c_2 = 5$ , which leads to a symmetric and computationally efficient weight function. The weight  $v(y; a, b)$  is zero for  $y \leq a$  and one for  $y \geq b$ , meaning that the left tail of the bGEV distribution is equal to the left tail in  $G$ , while the right tail is equal to the right tail in  $F$ . The choice of the weight  $v(y; a, b)$  should not considerably affect inference if we let the difference between  $a$  and  $b$  be small. The parameters  $\tilde{\mu}$  and  $\tilde{\sigma}$  are injective functions of  $(\mu, \sigma, \xi)$  such that the bGEV distribution function is continuous and  $F(y; \mu, \sigma, \xi) = G(y; \tilde{\mu}, \tilde{\sigma})$  for  $y \in \{a, b\}$ . Setting  $a = F^{-1}(p_a)$  and  $b = F^{-1}(p_b)$  with small probabilities  $p_a = 0.1$ ,  $p_b = 0.2$  makes it possible to model the right tail of the GEV distribution without any of the problems caused by a finite left tail. It may seem unnatural to model block maxima using the bGEV distribution when it is known that the correct limiting distribution is the GEV distribution. However, there is only a finite number of available observations, meaning that the GEV distribution is simply an approximation to the true distribution of the yearly maxima. In addition, when predicting large quantiles, our interest solely lies in the right tail of the bGEV distribution, which is identical to the right tail of the GEV distribution. Thus, the possibly less correct modelling of the left tail is a fair price to pay considering the improvements in terms of inference and the possible problems caused by overestimated lower bounds for the GEV distribution.

Naturally, the bGEV distribution can only be applied for modelling heavy-tailed phenomena ( $\xi \geq 0$ ). However, it is well established that extreme precipitation should be modelled with a non-negative tail parameter. Cooley et al. (2007) performs Bayesian spatial modelling of extreme daily precipitation in Colorado and find that the tail parameter is positive and less than 0.15. Papalexiou and Koutsoyiannis (2013) examine more than 15000 records of daily precipitation worldwide and conclude that the Fréchet distribution performs the best. They propose that even when the data suggests a negative tail parameter, it is more reasonable to use a Gumbel or Fréchet distribution. Less information is available concerning the distribution of extreme sub-daily precipitation. However, Koutsoyiannis et al. (1998) argues that the

distribution of precipitation should not have an upper bound for any aggregation period, so  $\xi$  must be non-negative. Van de Vyver (2012) estimate the distribution of yearly precipitation maxima in Belgium for aggregation times down to 1 minute, and find that the estimates of  $\xi$  increase as the aggregation times decreases, meaning that the tail parameter for sub-daily precipitation should be larger than for daily precipitation. Dyrddal et al. (2016) estimate  $\xi$  for daily precipitation in Norway from the seNorge1 data product (Mohr, 2009; Tveito et al., 2005) and conclude that the tail parameter estimates are non-constant in space and often negative. However, the authors do not provide confidence intervals or p-values and do not state whether the estimates are significantly different from zero. Based on our own exploratory analysis (results not shown) and the overwhelming evidence in the literature, we assume that sub-daily precipitation is a heavy-tailed phenomenon.

Following Castro-Camilo et al. (2021), we reparametrise the bGEV distribution from  $(\mu, \sigma, \xi)$  to  $(\mu_\alpha, \sigma_\beta, \xi)$ , where the location parameter  $\mu_\alpha$  is equal to the  $\alpha$  quantile of the bGEV distribution if  $\alpha \geq p_b$ . The scale parameter  $\sigma_\beta$ , hereby denoted the spread parameter, is equal to the difference between the  $1 - \beta/2$  quantile and the  $\beta/2$  quantile of the bGEV distribution if  $\beta/2 \geq p_b$ . There is a one to one relationship between the new and the old parameters. The new parametrisation is advantageous as it is considerably easier to interpret than the old parametrisation. The parameters  $\mu_\alpha$  and  $\sigma_\beta$  are directly connected to the quantiles of the bGEV distribution, whereas  $\mu$  and  $\sigma$  have no simple connections with any kind of moments or quantiles. Consequently, it is much easier to choose informative priors for  $\mu_\alpha$  and  $\sigma_\beta$ . Based on preliminary experiments, we find that  $\alpha = 0.5$  and  $\beta = 0.8$  are good choices that makes it easy to select informative priors. This is because the empirical quantiles close to the median have less variance. We have also experienced that R-INLA is more numerically stable when the spread is small, i.e.  $\beta$  is large.

### 3.2 Models

Let  $y_t(\mathbf{s})$  denote the maximum precipitation at location  $\mathbf{s} \in \mathcal{S}$  during year  $t \in \mathcal{T}$ , where  $\mathcal{S}$  is the study area and  $\mathcal{T}$  is the time period in focus. We assume a bGEV distribution for the yearly precipitation maxima,

$$[y_t(\mathbf{s}) | \mu_\alpha(\mathbf{s}), \sigma_\beta(\mathbf{s}), \xi(\mathbf{s})] \sim \text{bGEV}(\mu_\alpha(\mathbf{s}), \sigma_\beta(\mathbf{s}), \xi(\mathbf{s})),$$

where all observations are assumed to be conditionally independent given the parameters  $\mu_\alpha(\mathbf{s})$ ,  $\sigma_\beta(\mathbf{s})$  and  $\xi(\mathbf{s})$ . Correct estimation of the tail parameter is a difficult problem which highly affects estimates of large quantiles. In order to simplify estimation, the tail parameter is assumed to be constant, i.e.  $\xi(\mathbf{s}) = \xi$ . This is a common procedure, as inference for  $\xi$  is difficult with little data (e.g. Opitz et al., 2018; Sang & Gelfand, 2009). The tail parameter is further restricted such that  $\xi < 0.5$ , resulting in a finite mean and variance for the yearly maxima. This restriction makes inference much easier and more numerically stable. Exploratory analysis of our data supports the hypothesis of a spatially constant  $\xi < 0.5$  and spatially varying  $\mu_\alpha(\mathbf{s})$  and  $\sigma_\beta(\mathbf{s})$  (results not shown). Two competing models are constructed for describing the spatial structure of  $\mu_\alpha(\mathbf{s})$  and  $\sigma_\beta(\mathbf{s})$ .



### 3.2.1 The joint model

In the first model, denoted the joint model, both parameters are modelled using linear combinations of explanatory variables. Additionally, to draw strength from neighbouring stations, a spatial Gaussian random field is added to the location parameter. This gives the model

$$\begin{aligned} [y_t(\mathbf{s}) | \mu_\alpha(\mathbf{s}), \sigma_\beta(\mathbf{s}), \xi] &\sim \text{bGEV}(\mu_\alpha(\mathbf{s}), \sigma_\beta(\mathbf{s}), \xi), \\ \mu_\alpha(\mathbf{s}) &= \mathbf{x}_\mu(\mathbf{s})^T \boldsymbol{\beta}_\mu + u_\mu(\mathbf{s}), \\ \log(\sigma_\beta(\mathbf{s})) &= \mathbf{x}_\sigma(\mathbf{s})^T \boldsymbol{\beta}_\sigma, \end{aligned} \tag{3}$$

where  $\mathbf{x}_\mu(\mathbf{s})$  and  $\mathbf{x}_\sigma(\mathbf{s})$  are vectors containing an intercept plus the explanatory variables described in Table 1, and  $\boldsymbol{\beta}_\mu$  and  $\boldsymbol{\beta}_\sigma$  are vectors of regression coefficients. The term  $u_\mu(\mathbf{s})$  is a zero-mean Gaussian field with Matérn correlation function, i.e.,

$$\text{Corr}(u_\mu(\mathbf{s}_i), u_\mu(\mathbf{s}_j)) = \frac{1}{2^{\nu-1}\Gamma(\nu)} \left( \sqrt{8\nu} \frac{d(\mathbf{s}_i, \mathbf{s}_j)}{\rho} \right)^\nu K_\nu \left( \sqrt{8\nu} \frac{d(\mathbf{s}_i, \mathbf{s}_j)}{\rho} \right).$$

Here,  $d(\mathbf{s}_i, \mathbf{s}_j)$  is the Euclidean distance between  $\mathbf{s}_i$  and  $\mathbf{s}_j$ ,  $\rho > 0$  is the range parameter and  $\nu > 0$  is the smoothness parameter. The function  $K_\nu$  is the modified Bessel function of the second kind and order  $\nu$ . The Matérn family is a widely used class of covariance functions in spatial statistics due to its flexible local behaviour and attractive theoretical properties (Guttorp & Gneiting, 2006; Matérn, 1986; Stein, 1999). Its form also naturally appears as the covariance function of some models for the spatial structure of point rain rates (Sun et al., 2015). Efficient inference for high-dimensional Gaussian random fields can be achieved using the SPDE approach of Lindgren et al. (2011), which is implemented in R-INLA. It is common to fix the smoothness parameter  $\nu$  instead of estimating it, as the parameter is difficult to identify from data. The SPDE approximation in R-INLA allows for  $0 < \nu \leq 1$ . We choose  $\nu = 1$  as this reflects our beliefs about the smoothness of the underlying physical process. Additionally, Whittle (1954) argues that  $\nu = 1$  is a more natural choice for spatial models than the less smooth exponential correlation function ( $\nu = 1/2$ ), and  $\nu = 1$  is also the most extensively tested value when using R-INLA with the SPDE approach (Lindgren & Rue, 2015).

The joint model is similar to the models of Davison et al. (2012), Dyrddal et al. (2015), and Geirsson et al. (2015). However, they all place a Gaussian random field in the linear predictor for the log-scale and for the tail parameter. Within the R-INLA framework, it is not possible to model the spread or the tail using Gaussian random fields. Based on the amount of available data and the difficulty of estimating the spread and tail parameters, we also believe that the addition of a spatial Gaussian field in either parameter would simply complicate parameter estimation without any considerable contributions to model performance. Consequently, we do not include any Gaussian random field in the spread or tail of the bGEV distribution.

### 3.2.2 The two-step model

The second model is specifically tailored for sparse data with large block sizes. In such data-sparse situations, a large observation at a single location can be explained by a large tail parameter or a large spread parameter. In practice this might cause identifiability issues

between  $\sigma_\beta(\mathbf{s})$  and  $\xi$ , even though the parameters are identifiable in theory. In order to put a flexible model on the spread while avoiding such issues, Vandeskog et al. (2021) propose a model which borrows strength from the peaks over threshold method for separate modelling of  $\sigma_\beta(\mathbf{s})$ .

For some large enough threshold  $x_{thr}(\mathbf{s})$ , the distribution of sub-daily precipitation  $X(\mathbf{s})$  larger than  $x_{thr}(\mathbf{s})$  is assumed to follow a generalised Pareto distribution (Davison & Smith, 1990)

$$P(X(\mathbf{s}) > x_{thr}(\mathbf{s}) + x | X(\mathbf{s}) > x_{thr}(\mathbf{s})) = \left(1 + \frac{\xi x}{\zeta(\mathbf{s})}\right)^{-1/\xi},$$

with tail parameter  $\xi$  and scale parameter  $\zeta(\mathbf{s}) = \sigma(\mathbf{s}) + \xi(x_{thr}(\mathbf{s}) - \mu(\mathbf{s}))$ , where  $\mu(\mathbf{s})$  and  $\sigma(\mathbf{s})$  are the original GEV parameters from (1). Since  $\xi$  is assumed to be constant in space, all spatial variations in the bGEV distribution must stem from  $\mu(\mathbf{s})$  or  $\sigma(\mathbf{s})$ . We therefore assume that the difference  $x_{thr}(\mathbf{s}) - \mu(\mathbf{s})$  between the threshold and the location parameter is proportional to the scale parameter  $\sigma(\mathbf{s})$ . This assumption leads to the spread  $\sigma_\beta(\mathbf{s})$  being proportional to the standard deviation of all observations larger than the threshold  $x_{thr}(\mathbf{s})$ . Based on this assumption, it is possible to model the spatial structure of the spread parameter independently of the location and tail parameter. Denote

$$\sigma_\beta(\mathbf{s}) = \sigma_\beta^* \cdot \sigma^*(\mathbf{s}),$$

with  $\sigma_\beta^*$  a standardising constant and  $\sigma^*(\mathbf{s})$  the standard deviation of all observations larger than  $x_{thr}(\mathbf{s})$  at location  $\mathbf{s}$ . Conditional on  $\sigma^*(\mathbf{s})$ , the block maxima can be standardised as

$$y_t^*(\mathbf{s}) = y_t(\mathbf{s})/\sigma^*(\mathbf{s}).$$

The standardised block maxima have a bGEV distribution with a constant spread parameter,

$$[y_t^*(\mathbf{s}) | \mu_\alpha^*(\mathbf{s}), \sigma_\beta^*, \xi] \sim \text{bGEV}(\mu_\alpha^*(\mathbf{s}), \sigma_\beta^*, \xi),$$

where  $\mu_\alpha^*(\mathbf{s}) = \mu_\alpha(\mathbf{s})/\sigma^*(\mathbf{s})$ . Consequently, the second model is divided into two steps. First, we model the standard deviation of large observations at all locations. Second, we standardise the block maxima observations and model the remaining parameters of the bGEV distribution. We denote this as the two-step model. The two-step model shares some similarities with regional frequency analysis (Carreau et al., 2016; Dalrymple, 1960; Hosking & Wallis, 1997; Naveau et al., 2014), which is a multi-step procedure where the data are standardised and pooled together inside homogeneous regions. However, we standardise the data differently and do not pool together data from different locations. Instead, we borrow strength from nearby locations by adding a spatial Gaussian random fields to our model and by keeping  $\xi$  constant for all locations.

The location parameter  $\mu_\alpha^*(\mathbf{s})$  is modelled as a linear combination of explanatory variables  $\mathbf{x}_\mu(\mathbf{s})$  and a Gaussian random field  $u_\mu(\mathbf{s})$ , just as  $\mu_\alpha(\mathbf{s})$  in the joint model (3). For estimation of  $\sigma^*(\mathbf{s})$ , the threshold  $x_{thr}(\mathbf{s})$  is chosen as the 99% quantile of all observed precipitation at location  $\mathbf{s}$ . The precipitation observations larger than  $x_{thr}(\mathbf{s})$  are declustered to account for temporal dependence, and only the cluster maximum of an exceedance is used for estimating  $\sigma^*(\mathbf{s})$ . This might sound counter-intuitive, as the aim of the two-step model is to use more data to simplify inference. However, even when only using the cluster maxima, inference

is less wasteful than for the joint model. By using all threshold exceedances for estimating  $\sigma^*(\mathbf{s})$ , we would need to account for the dependence within exceedance clusters, which would add another layer of complexity to the modelling procedure. Consequently, we have chosen to not model the temporal dependence and only use the cluster-maxima for inference in this paper. To avoid high uncertainty from locations with few observations,  $\sigma^*(\mathbf{s})$  is only computed at stations with more than three years of data. In order to estimate  $\sigma^*(\mathbf{s})$  at locations with little or no observations, a linear regression model is used, where the logarithm of  $\sigma^*(\mathbf{s})$  is assumed to have a Gaussian distribution,

$$[\log(\sigma^*(\mathbf{s})) | \eta(\mathbf{s}), \tau] \sim \mathcal{N}(\eta(\mathbf{s}), \tau^{-1}),$$

with precision  $\tau$  and mean  $\eta(\mathbf{s}) = \mathbf{x}_\sigma(\mathbf{s})^T \boldsymbol{\beta}_\sigma$ . The estimated posterior mean from the regression model is then used as an estimator for  $\sigma^*(\mathbf{s})$  at all locations. Consequently, the complete two-step model is given as

$$\begin{aligned} [\log(\sigma^*(\mathbf{s})) | \eta(\mathbf{s}), \tau] &\sim \mathcal{N}(\eta(\mathbf{s}), \tau^{-1}), \\ \eta(\mathbf{s}) &= \mathbf{x}_\sigma(\mathbf{s})^T \boldsymbol{\beta}_\sigma, \\ [y_t^*(\mathbf{s}) | \mu_\alpha^*(\mathbf{s}), \sigma_\beta^*, \xi] &\sim \text{bGEV}(\mu_\alpha^*(\mathbf{s}), \sigma_\beta^*, \xi), \\ y_t^*(\mathbf{s}) &= y_t(\mathbf{s}) / \sigma^*(\mathbf{s}), \\ \mu_\alpha^*(\mathbf{s}) &= \mathbf{x}_\mu(\mathbf{s})^T \boldsymbol{\beta}_\mu + u_\mu(\mathbf{s}). \end{aligned} \tag{4}$$

Notice that the formulation of the two-step model makes it trivial to add more complex components for modelling the spread. One can, therefore, easily add a spatial Gaussian random field to the linear predictor of  $\log(\sigma^*(\mathbf{s}))$  while still using the R-INLA framework for inference, which is not possible with the joint model. In Section 4 we perform modelling both with and without a Gaussian random field in the spread to test how it affects model performance.

The uncertainty in the estimator for  $\sigma^*(\mathbf{s})$  is not propagated into the bGEV model for the standardised response, meaning that the estimated uncertainties from the two-step model are likely to be too small. This can be corrected with a bootstrapping procedure, where we draw  $B$  samples from the posterior of  $\log(\sigma^*(\mathbf{s}))$  and estimate  $(\mu_\alpha^*(\mathbf{s}), \sigma_\beta^*, \xi)$  for each of the  $B$  samples. Vandeskog et al. (2021) show that the two-step model with 100 bootstrap samples is able to outperform the joint model in a simple setting.

It might seem contradictory to employ a model based on exceedances in our setting, since we claim that the data quality is too bad to use the peaks over threshold model for estimating return levels. However, merely estimating the standard deviation of all threshold exceedances is a much simpler task than to estimate spatially varying parameters of the generalised Pareto distribution, including the tail parameter  $\xi$ . Thus, while we claim that the available data is not of good enough quality to estimate return levels in a similar fashion to Opitz et al. (2018), we also claim that it is of good enough quality to perform the simple task of estimating the trends in the spread parameter. The estimation of all remaining parameters, including  $\xi$ , is performed using block maxima data, which we believe to be of better quality.

### 3.3 INLA

By placing a Gaussian prior on  $\beta_\mu$ , both the joint and the two-step models fall into the class of latent Gaussian models. This is advantageous as it allows for inference using INLA with the R-INLA library (Bivand et al., 2015; Rue et al., 2009; Rue et al., 2017). The extreme value framework is quite new to the R-INLA package. Still, in recent years, some papers have started to appear where it is used for modelling extremes with INLA (e.g. Castro-Camilo et al., 2019; Opitz et al., 2018). R-INLA includes an implementation of the SPDE approximation for Gaussian random fields with a Matérn correlation function, which is used on the random field  $u_\mu(\mathbf{s})$  for a considerable improvement in inference speed.

A requirement for using INLA is that the model likelihood is log-concave. Unfortunately, neither the GEV distribution nor the bGEV distribution have log-concave likelihoods when  $\xi > 0$ . This can cause severe problems for model inference. However, we find that these problems are mitigated by choosing slightly informative priors for the model parameters, which is possible because of the reparametrisation described in Section 3.1. Additionally, we find that R-INLA is more stable when given a response that is standardised such that the difference between its 95% quantile and its 5% quantile is equal to 1. Based on the authors' experience, similar standardisation of the response is also a common procedure when using INLA for estimating the Weibull distribution parameters within the field of survival analysis. We believe that the combination of slightly informative priors and standardisation of the response is enough to fix the problems of non-concavity and ensure that R-INLA is working well with the bGEV distribution.

### 3.4 Evaluation

Model performance can be evaluated using the continuous ranked probability score (CRPS; Friederichs & Thorarinsdottir, 2012; Gneiting & Raftery, 2007; Matheson & Winkler, 1976),

$$\text{CRPS}(F, y) = \int_{-\infty}^{\infty} (F(t) - I(t \geq y))^2 dt = 2 \int_0^1 \ell_p(y - F^{-1}(p)) dp, \quad (5)$$

where  $F$  is the forecast distribution,  $y$  is an observation,  $\ell_p(x) = x(p - I(x < 0))$  is the quantile loss function and  $I(\cdot)$  is an indicator function. The CRPS is a strictly proper scoring rule, meaning that the expected value of  $\text{CRPS}(F, y)$  is minimised for  $G = F$  if and only if  $y \sim G$ . The importance of proper scoring rules when forecasting extremes is discussed by Lerch et al. (2017). From (5), one can see that the CRPS is equal to the integral over the quantile loss function for all possible quantiles. However, we are only interested in predicting large quantiles, and the model performance for small quantiles is of little importance to us. The threshold weighted CRPS (twCRPS; Gneiting & Ranjan, 2011) is a modification of the CRPS that allows for emphasis on specific areas of the forecast distribution,

$$\text{twCRPS}(F, y) = 2 \int_0^1 \ell_p(y - F^{-1}(p)) w(p) dp, \quad (6)$$

where  $w(p)$  is a non-negative weight function. A possible choice of  $w(p)$  for focusing on the right tail is the indicator function  $w(p) = I(p > p_0)$ . As described by Bolin and Wallin (2019),

the mean twCRPS is not robust to outliers and it gives more weight to forecast distributions with large variances, i.e. at locations far away from any weather station. A scaled version of the twCRPS, denoted the StwCRPS, is created using theorem 5 of Bolin and Wallin (2019):

$$S_{\text{scaled}}(F, y) = \frac{S(F, y)}{|S(F, F)|} + \log(|S(F, F)|), \quad (7)$$

where  $S(F, y)$  is the twCRPS and  $S(F, F)$  is its expected value with respect to the forecast distribution,

$$S(F, F) = \int S(F, y) dF(y).$$

The mean StwCRPS is more robust to outliers and varying degrees of uncertainty in forecast distributions, while still being a proper scoring rule (Bolin & Wallin, 2019).

Using R-INLA we are able to sample from the posterior distribution of the bGEV parameters at any location  $\mathbf{s}$ . The forecast distribution at location  $\mathbf{s}$  is therefore given as

$$\hat{F}_{\mathbf{s}}(\cdot) = \frac{1}{m} \sum_{i=1}^m F(\cdot; \mu_{\alpha}^{(i)}(\mathbf{s}), \sigma_{\beta}^{(i)}(\mathbf{s}), \xi^{(i)}), \quad (8)$$

where  $F$  is the distribution function of the bGEV distribution and  $(\mu_{\alpha}^{(i)}(\mathbf{s}), \sigma_{\beta}^{(i)}(\mathbf{s}), \xi^{(i)})$  are drawn from the posterior distribution of the bGEV parameters for  $i = 1, \dots, m$ , where  $m$  is a multiple of the number  $B$  of bootstrap samples. A closed-form expression is not available for the twCRPS when using the forecast distribution from (8). Consequently, we evaluate the twCRPS and StwCRPS using numerical integration.

## 4 Modelling sub-daily precipitation extremes in Norway

The models from Section 3 are applied for estimating return levels in the south of Norway. Table 1 shows which explanatory variables are used for modelling the location and spread parameters in both models. All explanatory variables are standardised to have zero mean and a standard deviation of 1, before being applied for modelling. Inference for the two-step model is performed both with and without propagation of the uncertainty in  $\sigma^*(\mathbf{s})$ . The uncertainty propagation is achieved using 100 bootstrap samples, as described in Section 3.2.2. Additionally, we modify the two-step model and add a random Gaussian field  $u_{\sigma}(\mathbf{s})$  to the linear predictor of the log-spread, to test if this can yield any considerable improvement in model performance. Just as  $u_{\mu}(\mathbf{s})$ ,  $u_{\sigma}(\mathbf{s})$  has zero mean and a Matérn covariance function.

### 4.1 Prior selection

Priors must be specified before we can model the precipitation extremes. From construction, the location parameter  $\mu_{\alpha}$  is equal to the  $\alpha$  quantile of the bGEV distribution. This allows us to place a slightly informative prior on  $\beta_{\mu}$ , using quantile regression on  $y^*(\mathbf{s})$  (Koenker, 2005, 2020). We choose a Gaussian prior for  $\beta_{\mu}$ , centred at the  $\alpha$  quantile regression estimates and

with a precision of 10. There is no unit on the precision in  $\beta_\mu$  because the block maxima have been standardised, as described in Section 3.3. The regression coefficients  $\beta_\sigma$  differ between the two-step and joint models. In the joint model, all the coefficients in  $\beta_\sigma$ , minus the intercept coefficient, are given Gaussian priors with zero mean and a precision of  $10^{-3}$ . The intercept coefficient, here denoted  $\beta_{0,\sigma}$ , is given a log-gamma prior with parameters such that  $\exp(\beta_{0,\sigma})$  has a gamma prior with mean equal to the empirical difference between the  $1 - \beta/2$  quantile and the  $\beta/2$  quantile of the standardised block maxima. The precision of the gamma prior is 10. In the two-step model, all coefficients of  $\beta_\sigma$  are given Gaussian priors with zero mean and a precision of  $10^{-3}$ , while the logarithm of  $\sigma_\beta^*$  is given the same log-gamma prior as the intercept coefficient in the joint model.

The parameters of the Gaussian random fields  $u_\mu$  and  $u_\sigma$  are given penalised complexity (PC) priors. The PC prior is a weakly informative prior distribution, designed to punish model complexity by placing an exponential prior on the distance from some base model (Simpson et al., 2017). Fuglstad et al. (2019) develop a joint PC prior for the range  $\rho > 0$  and standard deviation  $\zeta > 0$  of a Gaussian random field, where the base model is defined to have infinite range and zero variance. The prior contains two penalty parameters, that can be decided by specifying the four parameters  $\rho_0$ ,  $\alpha_1$ ,  $\zeta_0$  and  $\alpha_2$  such that  $P(\rho < \rho_0) = \alpha_1$  and  $P(\zeta > \zeta_0) = \alpha_2$ . We choose  $\alpha_1 = \alpha_2 = 0.05$ .  $\rho_0$  is given a value of 75 km for both the random fields, meaning that we place a 95% probability on the range being larger than 75 km. To put this range into context, the study area has a dimension of approximately  $730 \times 460$  km<sup>2</sup>, and the mean distance from one station to its closest neighbour is 10 km.  $\zeta_0$  is given a value of 0.5 mm for  $u_\sigma$ , meaning that we place a 95% probability on the standard deviation being smaller than 0.5 mm. This seems to be a reasonable value because the estimated logarithm of  $\sigma^*(\mathbf{s})$  lies in the range between 0.1 mm and 3.5 mm for all available weather stations and all examined aggregation times. For  $u_\mu$  we set  $\zeta_0 = 0.5$ , which is a reasonable value because of the standardisation of the response described in Section 3.3.

A PC prior is also placed on the tail parameter  $\xi$ . Opitz et al. (2018) develop a PC prior for the tail parameter of the generalised Pareto distribution, which is the default prior for  $\xi$  in R-INLA when modelling with the bGEV distribution. However, to the best of our knowledge, expressions for the PC priors for  $\xi$  in the GEV or bGEV distributions are not previously available in the literature. In Appendix A we develop expressions for the PC prior of  $\xi \in [0, 1)$  with base model  $\xi = 0$  for the GEV distribution and the bGEV distribution. Closed-form expressions do not exist, but the priors can be approximated numerically. Having computed the PC priors for the GEV distribution and the bGEV distribution, we find that they are similar to the PC prior of the generalised Pareto distribution. Consequently, we choose to model the tail parameter of the bGEV distribution with the PC prior for the generalised Pareto distribution (Opitz et al., 2018):

$$\pi(\xi) = \frac{\lambda}{\sqrt{2}} \exp \left( -\frac{\lambda}{\sqrt{2}} \frac{\xi}{(1 - \xi)^{1/2}} \right) \left( \frac{1 - \xi/2}{(1 - \xi)^{3/2}} \right),$$

with  $0 \leq \xi < 1$  and penalty parameter  $\lambda$ . Even though the prior is defined for values of  $\xi$  up to 1, a reparametrisation is performed within R-INLA such that  $0 \leq \xi < 0.5$ . Since the base model has  $\xi = 0$ , the prior places more weight on small values of  $\xi$  when  $\lambda$  increases. Based on the plots in Figure A.1 we find a value of  $\lambda = 7$  to give a good description of our prior beliefs, as we expect  $\xi$  to be positive but small.



Table 2: Mean StwCRPS with weight function  $w(p) = I(p > 0.9)$  for 5-fold cross-validation performed using out-of-sample estimation and in-sample estimation. The two-step method is tested with and without a Gaussian field in the spread and bootstrapping for propagation of uncertainty. Cross-validation is performed for precipitation aggregated over periods of 1 hour, 3 hours, 6 hours, 12 hours and 24 hours. The best scores are written in **bold**.

	Model	$u_\sigma(\mathbf{s})$	Boot- strap	1 h	3 h	6 h	12 h	24 h
Out-of- sample	Joint			−0.872	−0.597	−0.412	−0.149	0.0502
	Two-step	✓	✓	−0.901	<b>−0.599</b>	<b>−0.423</b>	−0.201	<b>0.0482</b>
	Two-step	✓		−0.893	−0.585	−0.414	−0.197	0.0630
	Two-step		✓	<b>−0.901</b>	−0.599	−0.423	<b>−0.201</b>	0.0482
	Two-step			−0.872	−0.583	−0.417	−0.196	0.0668
In- sample	Joint			−0.876	−0.608	−0.445	−0.230	0.0204
	Two-step	✓	✓	−1.003	−0.714	−0.564	−0.328	−0.1064
	Two-step	✓		<b>−1.012</b>	<b>−0.721</b>	<b>−0.577</b>	<b>−0.333</b>	<b>−0.1163</b>
	Two-step		✓	−1.003	−0.714	−0.565	−0.328	−0.1065
	Two-step			−0.886	−0.607	−0.454	−0.243	−0.0179

## 4.2 Cross-validation

Model performance is evaluated using five-fold cross-validation with the StwCRPS. The StwCRPS weight function is chosen as  $w(p) = I(p > 0.9)$ . Both in-sample and out-of-sample performance are evaluated. The mean StwCRPS over all five folds are displayed in Table 2. The two-step model outperforms the joint model for all aggregation times. When performing in-sample estimation, the variant of the two-step model with a Gaussian field and without bootstrapping always outperforms the other contestants. For out-of-sample estimation, the two variants of the two-step model that use bootstrapping attain very similar results, and they outperform all other models. The difference between in-sample estimation and out-of-sample estimation suggests that the two-step model overfits when the uncertainty in  $\sigma^*(\mathbf{s})$  is not correctly propagated into the modelling of  $(\mu_\alpha^*(\mathbf{s}), \sigma_\beta^*, \xi)$ . The difference in complexity between the two-step models with bootstrapping is quite considerable, as one model contains two spatial random fields, and the other only contains one. On the other hand, the model performance is practically identical. This demonstrates that there is little need for placing an overly complex model on the spread parameter. Consequently, for estimation of the bGEV parameters and return levels, we choose to use the two-step model with bootstrapping and without a spatial Gaussian random field in the spread.

### 4.3 Parameter estimates

The parameters of the two-step model are estimated for different aggregation times between 1 and 24 hours. Uncertainty is propagated using  $B = 100$  bootstrap samples. Estimation of the posterior of  $(\mu_\alpha^*(\mathbf{s}), \sigma_\beta^*, \xi)$  given some value of  $\sigma^*(\mathbf{s})$  takes less than 2 minutes on a 2.4 GHz laptop with 16 GB RAM, and the 100 bootstraps can be computed in parallel. On a moderately sized computational server, inference can thus be performed in well under 10 minutes.

The estimated values of the regression coefficients  $\beta_\mu$  and  $\beta_\sigma$ , and the standard deviation of the Gaussian field  $u_\mu(\mathbf{s})$ , are displayed in Table 3 for some selected temporal aggregations. These estimates are computed by drawing 20 samples from each of the  $B = 100$  posterior distributions. The empirical mean, standard deviation and quantiles of these 2000 samples are then reported. There is strong evidence that all the explanatory variables in  $\mathbf{x}_\sigma(\mathbf{s})$  are affecting the spread, with the northing being the most important explanatory variable. There is considerably less evidence that all our chosen explanatory variables have an effect on the location parameter. However, as the posterior distribution of  $\beta_\mu$  is estimated using 100 different samples from the posterior of  $\sigma^*(\mathbf{s})$ , it might be that the different regression coefficients are more significant for some of the standardisations, and less significant for others. The explanatory variable that has the greatest effect on the location parameter seems to be the mean annual precipitation. Thus, at locations with large amounts of precipitation, we expect the extreme precipitation to be heavier than at locations with little precipitation. From the estimates for  $\beta_\sigma$ , we also expect more variance in the distribution of extreme precipitation in the south. For a temporal aggregation of 1 hour, the standard deviation of  $u_\mu(\mathbf{s})$  is quite noticeable when compared to the regression coefficients  $\beta_\mu$ . However, as the temporal aggregation increases, the importance of the Gaussian field is considerably reduced.

Table 4 displays the posterior range of the  $u_\mu(\mathbf{s})$ . For the available data, the median number of neighbours within a radius of 50 km is 17, and the median number of neighbours within a radius of 100 km is 36. Based on these numbers, one can see that the Gaussian field is able to introduce spatial correlation between a large number of different stations. The range of the Gaussian field is considerably reduced as the temporal aggregation increases. It seems that, for 1 hour precipitation, the regression coefficients are unable to explain some kind of large-scale phenomenon that considerably affects the location parameter  $\mu_\alpha(\mathbf{s})$ . To correct this, both the range and standard deviation of  $u_\mu(\mathbf{s})$  have to be large. For longer aggregation periods, this phenomenon is not as important anymore, and the regression coefficients are able to explain most of the large-scale trends. Consequently, the range of  $u_\mu(\mathbf{s})$  is decreased, and its standard deviation becomes much smaller. The posterior means of  $u_\mu(\mathbf{s})$  for three different temporal aggregations are displayed over a  $1 \times 1$  km<sup>2</sup> gridded map in Figure 2. It is known that extreme precipitation dominates in the southeast of Norway for short aggregation times because of its large amount of convective precipitation (see, e.g. Dyrddal et al., 2015). Based on Figure 2 it becomes evident that our explanatory variables are unable to describe this regional difference when modelling hourly precipitation, and  $u_\mu(\mathbf{s})$  has to do the job of separating between the east and the west. This explains the large size of  $SD(u_\mu)$  for hourly precipitation, seen in Table 3. As the temporal aggregations increase from one hour to three and six hours, the difference between east and west diminishes, and it seems that

Table 3: Estimated regression coefficients  $\beta_\mu$ ,  $\beta_\sigma$  and estimated standard deviation  $SD(u_\mu)$  of the Gaussian field  $u_\mu(\mathbf{s})$  in the two-step model for yearly maximum precipitation at different temporal aggregations.

Temporal aggregation	Parameter	Explanatory variable	Mean	SD	2.5% quantile	50% quantile	97.5% quantile
1 hour	$\beta_\mu$	Intercept	0.669	0.066	0.518	0.675	0.794
		Mean annual precipitation	0.071	0.012	0.044	0.072	0.091
		Altitude	-0.006	0.011	-0.026	-0.006	0.013
		Easting	-0.044	0.035	-0.118	-0.042	0.017
		Northing	0.036	0.038	-0.036	0.036	0.111
		Distance to the open sea	-0.001	0.033	-0.072	0.002	0.055
	$SD(u_\mu)$		0.178	0.019	0.136	0.179	0.211
	$\beta_\sigma$	Intercept	0.916	0.013	0.891	0.916	0.941
		Easting	0.088	0.015	0.059	0.088	0.117
		Northing	-0.147	0.014	-0.175	-0.147	-0.120
		Distance to the open sea	-0.051	0.016	-0.082	-0.051	-0.020
3 hours	$\beta_\mu$	Intercept	0.847	0.025	0.800	0.846	0.895
		Mean annual precipitation	0.120	0.012	0.096	0.122	0.139
		Altitude	-0.009	0.009	-0.027	-0.010	0.007
		Easting	0.016	0.021	-0.025	0.017	0.057
		Northing	0.022	0.018	-0.015	0.024	0.054
		Distance to the open sea	0.017	0.018	-0.021	0.017	0.052
	$SD(u_\mu)$		0.090	0.016	0.057	0.089	0.120
	$\beta_\sigma$	Intercept	1.446	0.012	1.423	1.446	1.470
		Easting	0.031	0.014	0.004	0.031	0.058
		Northing	-0.135	0.013	-0.161	-0.135	-0.109
		Distance to the open sea	-0.057	0.015	-0.086	-0.057	-0.028
6 hours	$\beta_\mu$	Intercept	0.911	0.024	0.868	0.911	0.962
		Mean annual precipitation	0.148	0.013	0.123	0.150	0.168
		Altitude	-0.012	0.009	-0.029	-0.011	0.005
		Easting	0.040	0.021	-0.001	0.040	0.080
		Northing	0.008	0.019	-0.029	0.009	0.042
		Distance to the open sea	0.030	0.020	-0.011	0.031	0.067
	$SD(u_\mu)$		0.047	0.013	0.028	0.046	0.072
	$\beta_\sigma$	Intercept	1.776	0.013	1.751	1.776	1.801
		Easting	-0.032	0.014	-0.060	-0.032	-0.004
		Northing	-0.093	0.014	-0.120	-0.093	-0.066
		Distance to the open sea	-0.065	0.016	-0.096	-0.065	-0.035

Table 4: Estimated posterior mean and quantiles for the range  $\rho$  of the Gaussian field  $u_\mu(\mathbf{s})$  and the tail parameter  $\xi$  in the two-step model for yearly maximum precipitation at different temporal aggregations.

Parameter	Temporal aggregation	Mean	2.5% quantile	50% quantile	97.5% quantile
$\rho$ [km]	1 hour	235	34	255	478
	3 hours	78	39	75	147
	6 hours	60	32	57	104
	12 hours	84	31	83	145
	24 hours	55	32	50	105
$\xi$	1 hour	0.178	0.136	0.179	0.211
	3 hours	0.090	0.057	0.089	0.120
	6 hours	0.047	0.028	0.046	0.072
	12 hours	0.032	0.010	0.031	0.048
	24 hours	0.029	0.006	0.029	0.051

the explanatory variables do a better job of explaining the variance in the location parameter  $\mu_\alpha(\mathbf{s})$ .

The posterior distribution of  $\xi$  is also described in Table 4. The tail parameter seems to decrease quickly as the aggregation time increases, and it is practically constant for precipitation over longer periods than 12 hours. This makes sense given the observation of Barbero et al. (2019) that most 24 hour annual maximum precipitation comes from rainstorms with lengths of less than 15 hours. Thus, the tail parameter for 24 hour precipitation should be close to the tail parameter for 12 hour precipitation. For 12 hours and up, the tail parameter is so small that one may wonder if a Gumbel distribution would not have given a better fit to the data. However, this is not the case for the shorter aggregation times, where the tail parameter is considerably larger.

#### 4.4 Return levels

We use the two-step model for estimating large return levels for the yearly precipitation maxima. Posterior distributions of the 20 year return levels are estimated on a grid with resolution  $1 \times 1$  km<sup>2</sup>. The posterior means and the widths of the 95% credible intervals are displayed in Figure 3. For a period of 1 hour the most extreme precipitation is located southeast in Norway, while for longer periods, the extreme precipitation is moving over to the west coast. These results are expected since we know that the convective precipitation of the southeast dominates for short aggregation periods. At the same time, the southwest of Norway generally has more precipitation, making it the dominant region for longer aggregation times.

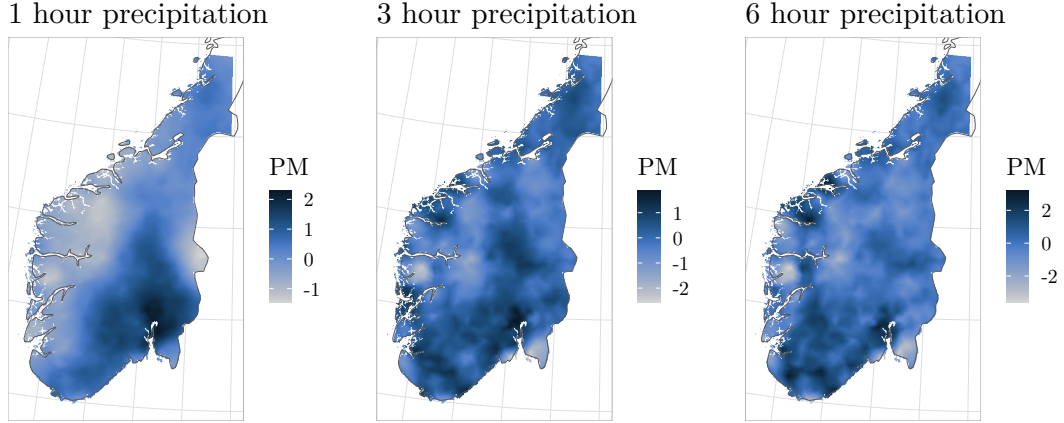


Figure 2: Estimated posterior mean (PM) of the Gaussian field  $u_\mu(\mathbf{s})$  for three different temporal aggregations of precipitation, with unit mm.

The spatial structure and magnitude of the 20 year return levels for hourly precipitation are similar to the estimates of Dyrddal et al. (2015), but with considerably thinner credible intervals. This makes sense as more data are available, and the two-step model is able to perform less wasteful inference. In addition, our model is much more simple, as they include a random Gaussian field in all three parameters, while we only include a random Gaussian field in the location parameter. This can also lead to less uncertainty in the return level estimates.

## 5 Conclusion

The blended generalised extreme value (bGEV) distribution is applied as a substitute for the generalised extreme value (GEV) distribution for estimation of the return levels of sub-daily precipitation in the south of Norway. The bGEV distribution simplifies inference by introducing a parameter-free support, but can only be applied for modelling of heavy-tailed phenomena. Sub-daily precipitation maxima are modelled using a spatial Bayesian hierarchical model with a latent Gaussian field. This is implemented using both integrated nested Laplace approximations (INLA) and the stochastic partial differential equation (SPDE) approach, for fast inference. Inference is also made more stable and less wasteful by our novel two-step modelling procedure that borrows strength from the peaks over threshold method when modelling block maxima. Like the GEV distribution, the bGEV distribution suffers from a lack of log-concavity, which can cause problems when using INLA. We are able to mitigate any problems caused by a lack of log-concavity by choosing slightly informative priors and standardising the data. We find that the bGEV distribution performs well as a model for extreme precipitation. The two-step model successfully utilises the additional information provided by the peaks over threshold data and is able to outperform models that

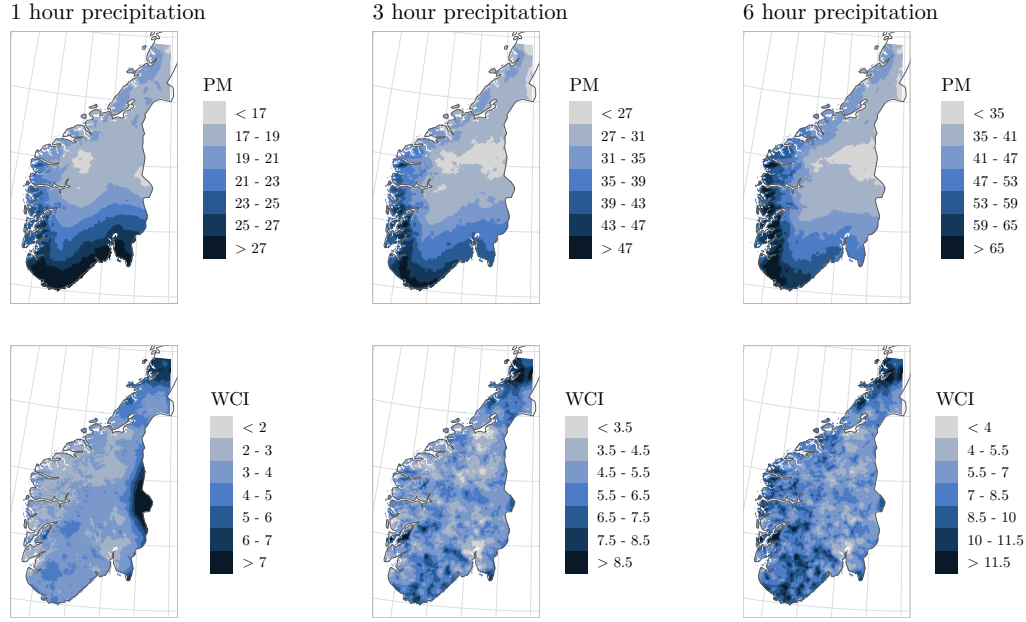


Figure 3: Estimated posterior mean (PM) and width of the 95% credible intervals (WCI) for the 20 year return levels of sub-daily precipitation. Different aggregation times are displayed in different columns. All numbers are given with unit mm.

only use block maxima data for inference.

## Acknowledgements

We thank Thordis L. Thorarinsdottir and Geir-Arne Fuglstad for helpful discussions.

## Funding

This publication is part of the World of Wild Waters (WoWW) project, which falls under the umbrella of Norwegian University of Science and Technology (NTNU)'s Digital Transformation initiative.

## Code and data availability

The necessary code and data for achieving these results are available online at <https://github.com/siliusmv/inlaBGEV>. The unprocessed data are freely available online, as described in Section 2.



# Conflicts of interest

The authors declare that they have no conflicts of interest.

## References

- Bakka, H., Rue, H., Fuglstad, G.-A., Riebler, A., Bolin, D., Illian, J., Krainski, E., Simpson, D., & Lindgren, F. (2018). Spatial modeling with R-INLA: A review. *WIREs Comput. Stat.*, 10(6), e1443. <https://doi.org/10.1002/wics.1443>
- Barbero, R., Fowler, H. J., Blenkinsop, S., Westra, S., Moron, V., Lewis, E., Chan, S., Lenderink, G., Kendon, E., Guerreiro, S., Li, X.-F., Villalobos, R., Ali, H., & Mishra, V. (2019). A synthesis of hourly and daily precipitation extremes in different climatic regions. *Weather Clim. Extremes*, 26, 100219. <https://doi.org/10.1016/j.wace.2019.100219>
- Bivand, R., Gómez-Rubio, V., & Rue, H. (2015). Spatial data analysis with R-INLA with some extensions. *Journal of Statistical Software*, 63(1), 1–31.
- Bolin, D., & Wallin, J. (2019). Scale dependence: Why the average CRPS often is inappropriate for ranking probabilistic forecasts. *arXiv:1912.05642*.
- Bücher, A., & Segers, J. (2017). On the maximum likelihood estimator for the generalized extreme-value distribution. *Extremes*, 20(4), 839–872. <https://doi.org/10.1007/s10687-017-0292-6>
- Bücher, A., & Segers, J. (2018). Inference for heavy tailed stationary time series based on sliding blocks. *Electronic Journal of Statistics*, 12(1), 1098–1125. <https://doi.org/10.1214/18-EJS1415>
- Bücher, A., & Zhou, C. (2021). A Horse Race Between the Block Maxima Method and the Peak-Over-Threshold Approach. *Statistical Science*, 36(3), 360–378. <https://doi.org/10.1214/20-STS795>
- Carreau, J., Naveau, P., & Neppel, L. (2016). Characterization of homogeneous regions for regional peaks-over-threshold modeling of heavy precipitation [working paper or preprint]. <https://hal.ird.fr/ird-01331374>
- Castro-Camilo, D., & Huser, R. (2020). Local likelihood estimation of complex tail dependence structures, applied to U.S. precipitation extremes. *J. Amer. Statist. Assoc.*, 115(531), 1037–1054. <https://doi.org/10.1080/01621459.2019.1647842>
- Castro-Camilo, D., Huser, R., & Rue, H. (2019). A spliced gamma-generalized Pareto model for short-term extreme wind speed probabilistic forecasting. *JABES*, 24(3), 517–534. <https://doi.org/10.1007/s13253-019-00369-z>
- Castro-Camilo, D., Huser, R., & Rue, H. (2021). Practical strategies for GEV-based regression models for extremes. *arXiv:2106.13110*.
- Coles, S. (2001). *An introduction to statistical modeling of extreme values*. Springer, London. <https://doi.org/10.1007/978-1-4471-3675-0>
- Cooley, D., Nychka, D., & Naveau, P. (2007). Bayesian spatial modeling of extreme precipitation return levels. *J. Amer. Statist. Assoc.*, 102(479), 824–840. <https://doi.org/10.1198/016214506000000780>
- Crespi, A., Lussana, C., Brunetti, M., Dobler, A., Maugeri, M., & Tveito, O. E. (2018). High-resolution monthly precipitation climatologies over Norway: Assessment of spatial interpolation methods. *arXiv:1804.04867*.
- Dalrymple, T. (1960). *Flood-frequency analyses*. U.S. Government Printing Office.
- Davison, A. C., & Huser, R. (2015). Statistics of extremes. *Annu. Rev. Stat. Appl.*, 2(1), 203–235. <https://doi.org/10.1146/annurev-statistics-010814-020133>
- Davison, A. C., Padoan, S. A., & Ribatet, M. (2012). Statistical modeling of spatial extremes. *Statist. Sci.*, 27(2), 161–186. <https://doi.org/10.1214/11-STS376>
- Davison, A. C., & Smith, R. L. (1990). Models for exceedances over high thresholds. *J. R. Stat. Soc. B*, 52(3), 393–425. <https://doi.org/10.1111/j.2517-6161.1990.tb01796.x>
- Dyrddal, A. V., Lenkoski, A., Thorarinsdottir, T. L., & Stordal, F. (2015). Bayesian hierarchical modeling of extreme hourly precipitation in Norway. *Environmetrics*, 26(2), 89–106. <https://doi.org/10.1002/env.2301>

- Dyrddal, A. V., Skaugen, T., Stordal, F., & Førland, E. J. (2016). Estimating extreme areal precipitation in Norway from a gridded dataset. *Hydrol. Sci. J.*, 61(3), 483–494. <https://doi.org/10.1080/02626667.2014.947289>
- Fisher, R. A., & Tippett, L. H. C. (1928). Limiting forms of the frequency distribution of the largest or smallest member of a sample. *Math. Proc. Cambridge Philos. Soc.*, 24(2), 180–190. <https://doi.org/10.1017/S0305004100015681>
- Friederichs, P., & Thorarinsdottir, T. L. (2012). Forecast verification for extreme value distributions with an application to probabilistic peak wind prediction. *Environmetrics*, 23(7), 579–594. <https://doi.org/10.1002/env.2176>
- Fuglstad, G.-A., Simpson, D., Lindgren, F., & Rue, H. (2019). Constructing priors that penalize the complexity of Gaussian random fields. *J. Amer. Statist. Assoc.*, 114(525), 445–452. <https://doi.org/10.1080/01621459.2017.1415907>
- Galassi, M., Davies, J., Theiler, J., Gough, B., Jungman, G., Alken, P., Booth, M., Rossi, F., & Ulerich, R. (2007). The GNU scientific library reference manual, 2007. <http://www.gnu.org/software/gsl>
- Geirsson, Ó. P., Hrafnkelsson, B., & Simpson, D. (2015). Computationally efficient spatial modeling of annual maximum 24-h precipitation on a fine grid. *Environmetrics*, 26(5), 339–353. <https://doi.org/10.1002/env.2343>
- Gneiting, T., & Raftery, A. E. (2007). Strictly proper scoring rules, prediction, and estimation. *J. Amer. Statist. Assoc.*, 102(477), 359–378. <https://doi.org/10.1198/016214506000001437>
- Gneiting, T., & Ranjan, R. (2011). Comparing density forecasts using threshold- and quantile-weighted scoring rules. *J. Bus. Econ. Stat.*, 29(3), 411–422. <https://doi.org/10.1198/jbes.2010.08110>
- Guttorp, P., & Gneiting, T. (2006). Studies in the History of Probability and Statistics XLIX on the Matérn Correlation family. *Biometrika*, 93(4), 989–995. <https://doi.org/10.1093/biomet/93.4.989>
- Hankin, R. K. S. (2006). Special functions in R: Introducing the Gsl package. *R News*, 6.
- Hanssen-Bauer, I., & Førland, E. J. (1998). Annual and seasonal precipitation variations in Norway 1896–1997. *DNMI KLIMA Report 27/98*.
- Hosking, J. R. M., & Wallis, J. R. (1997). *Regional frequency analysis*.
- Katz, R. W., Parlange, M. B., & Naveau, P. (2002). Statistics of extremes in hydrology. *Adv. Water Res.*, 25(8), 1287–1304. [https://doi.org/10.1016/S0309-1708\(02\)00056-8](https://doi.org/10.1016/S0309-1708(02)00056-8)
- Koenker, R. (2005). *Quantile regression* (Vol. 38). <https://doi.org/10.1017/CBO9780511754098>
- Koenker, R. (2020). *Quantreg: Quantile regression* [R package version 5.75]. <https://CRAN.R-project.org/package=quantreg>
- Koutsoyiannis, D., Kozonis, D., & Manetas, A. (1998). A mathematical framework for studying rainfall intensity-duration-frequency relationships. *Journal of Hydrology*, 206(1), 118–135. [https://doi.org/10.1016/S0022-1694\(98\)00097-3](https://doi.org/10.1016/S0022-1694(98)00097-3)
- Lehmann, E. A., Phatak, A., Stephenson, A., & Lau, R. (2016). Spatial modelling framework for the characterisation of rainfall extremes at different durations and under climate change. *Environmetrics*, 27(4), 239–251. <https://doi.org/10.1002/env.2389>
- Lerch, S., Thorarinsdottir, T. L., Ravazzolo, F., & Gneiting, T. (2017). Forecaster’s dilemma: Extreme events and forecast evaluation. *Statist. Sci.*, 32(1), 106–127. <https://doi.org/10.1214/16-STS588>
- Lindgren, F., & Rue, H. (2015). Bayesian spatial modelling with R-INLA. *J Stat Softw*, 63(19).
- Lindgren, F., Rue, H., & Lindström, J. (2011). An explicit link between Gaussian fields and Gaussian Markov random fields: The stochastic partial differential equation approach. *J. R. Stat. Soc. B*, 73(4), 423–498. <https://doi.org/10.1111/j.1467-9868.2011.00777.x>
- Lussana, C., Saloranta, T., Skaugen, T., Magnusson, J., Tveito, O. E., & Andersen, J. (2018). SeNorge2 daily precipitation, an observational gridded dataset over Norway from 1957 to the present day. *Earth Syst. Sci. Data*, 10(1), 235. <https://doi.org/10.5194/essd-10-235-2018>
- Lussana, C., Tveito, O., & Uboldi, F. (2018). Three-dimensional spatial interpolation of 2 m temperature over Norway. *Q. J. R. Meteorolog. Soc.*, 144(711), 344–364. <https://doi.org/10.1002/qj.3208>
- Matérn, B. (1986). *Spatial variation* (2nd ed. 1986., Vol. 36). Springer New York : Imprint: Springer. <https://doi.org/10.1007/978-1-4615-7892-5>
- Matheson, J. E., & Winkler, R. L. (1976). Scoring rules for continuous probability distributions. *Manage Sci*, 22(10), 1087–1096. <https://doi.org/10.1287/mnsc.22.10.1087>

- Mohr, M. (2009). Comparison of versions 1.1 and 1.0 of gridded temperature and precipitation data for Norway. *met.no note*, 19.
- Naveau, P., Toreti, A., Smith, I., & Xoplaki, E. (2014). A fast nonparametric spatio-temporal regression scheme for generalized Pareto distributed heavy precipitation. *Water Resources Research*, 50(5), 4011–4017. <https://doi.org/10.1002/2014WR015431>
- Opitz, T., Huser, R., Bakka, H., & Rue, H. (2018). INLA goes extreme: Bayesian tail regression for the estimation of high spatio-temporal quantiles. *Extremes*, 21(3), 441–462. <https://doi.org/10.1007/s10687-018-0324-x>
- Papalexiou, S. M., & Koutsoyiannis, D. (2013). Battle of extreme value distributions: A global survey on extreme daily rainfall. *Water Resour. Res.*, 49(1), 187–201. <https://doi.org/10.1029/2012WR012557>
- Robinson, M. E., & Tawn, J. A. (2000). Extremal analysis of processes sampled at different frequencies. *J. R. Stat. Soc. B*, 62(1), 117–135. <https://doi.org/10.1111/1467-9868.00223>
- Rue, H., Martino, S., & Chopin, N. (2009). Approximate Bayesian inference for latent Gaussian models by using integrated nested Laplace approximations. *J. R. Stat. Soc. B*, 71(2), 319–392. <https://doi.org/10.1111/j.1467-9868.2008.00700.x>
- Rue, H., Riebler, A., Sørbye, S. H., Illian, J. B., Simpson, D. P., & Lindgren, F. K. (2017). Bayesian computing with INLA: A review. *Annu. Rev. Stat. Appl.*, 4(1), 395–421. <https://doi.org/10.1146/annurev-statistics-060116-054045>
- Sang, H., & Gelfand, A. E. (2009). Hierarchical modeling for extreme values observed over space and time. *Environ. Ecol. Stat.*, 16(3), 407–426. <https://doi.org/10.1007/s10651-007-0078-0>
- Simpson, D., Rue, H., Riebler, A., Martins, T. G., & Sørbye, S. H. (2017). Penalising model component complexity: A principled, practical approach to constructing priors. *Statist. Sci.*, 32(1), 1–28. <https://doi.org/10.1214/16-STS576>
- Smith, R. L. (1985). Maximum likelihood estimation in a class of nonregular cases. *Biometrika*, 72(1), 67–90. <https://doi.org/10.1093/biomet/72.1.67>
- Stein, M. L. (1999). *Interpolation of spatial data : Some theory for Kriging*. Springer.
- Sun, Y., Bowman, K. P., Genton, M. G., & Tokay, A. (2015). A Matérn model of the spatial covariance structure of point rain rates. *Stoch Env Res Risk A*, 29(2), 411–416. <https://doi.org/10.1007/s00477-014-0923-2>
- Tveito, O. E., Bjørndal, I., Skjelvåg, A. O., & Aune, B. (2005). A GIS-based agro-ecological decision system based on gridded climatology. *Meteorol Appl*, 12(1), 57–68. <https://doi.org/10.1017/S1350482705001490>
- Ulrich, J., Jurado, O. E., Peter, M., Scheibel, M., & Rust, H. W. (2020). Estimating IDF curves consistently over durations with spatial covariates. *Water*, 12(11). <https://doi.org/10.3390/w12113119>
- Van de Vyver, H. (2012). Spatial regression models for extreme precipitation in Belgium. *Water Resour. Res.*, 48(9). <https://doi.org/10.1029/2011WR011707>
- Vandeskog, S. M., Martino, S., & Castro-Camilo, D. (2021). Modelling block maxima with the blended generalised extreme value distribution. *22nd European Young Statisticians Meeting - Proceedings*.
- Wang, Y., & So, M. K. (2016). A Bayesian hierarchical model for spatial extremes with multiple durations. *Computational Statistics & Data Analysis*, 95, 39–56. <https://doi.org/10.1016/j.csda.2015.09.001>
- Whittle, P. (1954). On stationary processes in the plane. *Biometrika*, 41(3/4), 434–449. <http://www.jstor.org/stable/2332724>
- Wilson, P. S., & Toumi, R. (2005). A fundamental probability distribution for heavy rainfall. *Geophys. Res. Lett.*, 32(14). <https://doi.org/10.1029/2005GL022465>
- World Economic Forum. (2021). *The global risks report 2021*. [http://www3.weforum.org/docs/WEF\\_The\\_Global\\_Risks\\_Report\\_2021.pdf](http://www3.weforum.org/docs/WEF_The_Global_Risks_Report_2021.pdf)
- Zou, N., Volgushev, S., & Bücher, A. (2019). Multiple block sizes and overlapping blocks for multivariate time series extremes. *arXiv:1907.09477*.

## A PC prior for the tail parameter

In order to compute the PC prior for the GEV and bGEV distribution with  $\xi \geq 0$  and base model  $\xi = 0$ , one must first compute  $\text{KLD}(\pi_\xi, \pi_0)$  for the GEV distribution and the bGEV distribution. Notice that the base model is identical for both distributions. Writing the GEV

distribution function as  $F(x) = \exp(-h(x))$  gives the probability density function

$$\pi_\xi(x) = -\exp(-h(x))h'(x), \quad h(x) = (1 + \xi(x - \mu)/\sigma)_+^{-1/\xi}.$$

The KLD for the GEV distribution is equal to

$$\begin{aligned} \text{KLD}(\pi_\xi, \pi_0) &= \int \pi_\xi(x) \log \left( \frac{\pi_\xi(x)}{\pi_0(x)} \right) dx \\ &= \int -e^{-h(x)}h'(x) \cdot \left( -h(x) + \log(-\sigma h'(x)) + \exp \left( -\frac{x - \mu}{\sigma} \right) + \frac{x - \mu}{\sigma} \right) dx. \end{aligned}$$

The fourth term of the KLD is simply equal to the expectation of  $(x - \mu)/\sigma$ , which is known. The first term is easily solvable with the substitution  $u = h(x)$ . Using the same substitution for the second term with the knowledge that  $\log(-\sigma h'(x)) = (1 + \xi) \log(h(x))$  gives the integral

$$\int -e^{-h(x)}h'(x) \log(-\sigma h'(x)) = \int_0^\infty e^{-u}(1 + \xi) \log(u) du = -(1 + \xi)\gamma,$$

where  $\gamma$  is the Euler-Mascheroni constant. We are unable to find a closed-form expression for the third term. However, using substitution with  $u = h(x)$  gives

$$\int -e^{-h(x)}h'(x) \exp \left( -\frac{x - \mu}{\sigma} \right) dx = \int_0^\infty \exp \left( \frac{1}{\xi} - u - \frac{u^{-\xi}}{\xi} \right) du.$$

With a change of variables, the integral in the KLD (A.1) is transformed to have finite limits,

$$\int_0^\infty \exp \left( \frac{1}{\xi} - (u + u^{-\xi}/\xi) \right) du = \int_0^1 \exp \left( \frac{1}{\xi} (1 - (-\log v)^{-\xi}) \right) dv.$$

This can easily be numerically approximated. Summarising, the KLD for the GEV is finite for  $\xi < 1$  and equal to

$$\text{KLD}(\pi_\xi, \pi_0) = -1 - (1 + \xi)\gamma + \xi^{-1}(\Gamma(1 - \xi) - 1) + \int_0^1 \exp \left( \frac{1}{\xi} (1 - (-\log v)^{-\xi}) \right) dv, \quad (\text{A.1})$$

where  $\Psi(\cdot)$  is the digamma function.

The PC prior has probability density function  $\pi(d) = \lambda \exp(-\lambda d)$  with the distance  $d = \sqrt{2\text{KLD}(\pi_\xi, \pi_0)}$ . Transforming the PC prior from a distribution on  $d$  to a distribution on  $\xi$  gives

$$\pi(\xi) = \lambda \exp(-\lambda d(\xi)) \left| \frac{\partial d(\xi)}{\partial \xi} \right| = \frac{\lambda}{d(\xi)} \exp(-\lambda d(\xi)) \left| \frac{\partial}{\partial \xi} \text{KLD}(\pi_\xi, \pi_0) \right|. \quad (\text{A.2})$$

Consequently, the derivative of the KLD must also be computed. Using derivation under the integral sign gives

$$\frac{\partial}{\partial \xi} \text{KLD}(\pi_\xi, \pi_0) = -\gamma - \frac{\Gamma(1 - \xi)\Psi(1 - \xi)}{\xi} - \frac{\Gamma(1 - \xi) - 1}{\xi^2} + \int_0^1 g(v; \xi) dv,$$

with

$$g(v; \xi) = \exp \left( \frac{1}{\xi} (1 - (-\log v)^{-\xi}) \right) \frac{1}{\xi^2} (-1 + (-\log v)^{-\xi} (1 + \xi \log(-\log v))) .$$

This integral must also be numerically approximated.

When computing the KLD for the bGEV distribution, the integral for the KLD is divided into three parts:

$$\begin{aligned} \text{KLD}(\pi_\xi, \pi_0) &= \\ & \int_{-\infty}^{p_a} \pi_\xi(x) \log \left( \frac{\pi_\xi(x)}{\pi_0(x)} \right) dx + \int_{p_a}^{p_b} \pi_\xi(x) \log \left( \frac{\pi_\xi(x)}{\pi_0(x)} \right) dx + \int_{p_b}^{\infty} \pi_\xi(x) \log \left( \frac{\pi_\xi(x)}{\pi_0(x)} \right) dx \\ &= \text{KLD}_{\text{Gumbel}}(\pi_\xi, \pi_0) + \text{KLD}_{\text{Blending}}(\pi_\xi, \pi_0) + \text{KLD}_{\text{Fréchet}}(\pi_\xi, \pi_0). \end{aligned}$$

A closed-form expression can be found for the Gumbel part of the KLD, where we express the Gumbel distribution function as  $G(x) = \exp(-h_2(x))$  and use the same substitution techniques as for the KLD computations with the GEV distribution. We get

$$\begin{aligned} \text{KLD}_{\text{Gumbel}}(\pi_\xi, \pi_0) &= \\ & -\Gamma_u(-\log p_a; 2) + p_a \log(-\log p_a) - E_i(\log p_a) + \Gamma_u(-\log p_a; C_1 + 1)e^{-C_2} \\ & - C_1 (p_a \log(-\log p_a) - E_i(\log p_a)) + p_a \left( C_2 + \log \xi + \log \left( \log \left( \frac{\log p_a}{\log p_b} \right) \right) \right) \\ & - p_a \log \left( (-\log p_b)^{-\xi} - (-\log p_a)^{-\xi} \right), \end{aligned}$$

where

$$C_1 = \frac{1}{\xi} \frac{(-\log p_b)^{-\xi} - (-\log p_a)^{-\xi}}{\log \left( \frac{\log p_a}{\log p_b} \right)} \quad \text{and} \quad C_2 = C_1 \log(-\log p_a) + \frac{1}{\xi} \left( (-\log p_a)^{-\xi} - 1 \right).$$

Here,  $\Gamma_u(x; \alpha) = \int_x^\infty t^{\alpha-1} e^{-t} dt$  is the upper incomplete gamma function, and  $E_i(x) = \int_{-\infty}^x (e^t/t) dt$  is the exponential integral, which can be evaluated using the GNU Scientific Library (Galassi et al., 2007; Hankin, 2006). The Fréchet part of the KLD is found in the same way as (A.1), only using different integration limits. For  $0 \leq \xi < 1$  we get

$$\begin{aligned} \text{KLD}_{\text{Fréchet}}(\pi_\xi, \pi_0) &= -\Gamma_l(-\log p_b; 2) + (\xi + 1) (-p_b \log(-\log p_b) + E_i(\log p_b) - \gamma) \\ & + \frac{1}{\xi} (\Gamma_l(-\log p_b; 1 - \xi) - (1 - p_b)) + \int_{p_b}^1 \exp \left( \frac{1}{\xi} (1 - (-\log u)^{-\xi}) \right) du, \end{aligned}$$

where  $\Gamma_l(x; \alpha) = \Gamma(\alpha) - \Gamma_u(x; \alpha)$  is the lower incomplete gamma function. The integral in the expression above must once again be evaluated numerically. We are unable to find an expression for the KLD integral between the  $p_a$  quantile and the  $p_b$  quantile. Thus, we use numerical integration with  $\mu = 1$  and  $\sigma = 0$  to compute  $\text{KLD}_{\text{Blending}}(\pi_\xi, \pi_0)$ . The value of the integral does not depend on the values of  $\mu$  and  $\sigma$ , but we are unable to compute it without choosing some value for them. Being unable to find an expression for the KLD of the bGEV distribution, we must also use numerical derivation to estimate the derivative of the KLD, needed in (A.2).

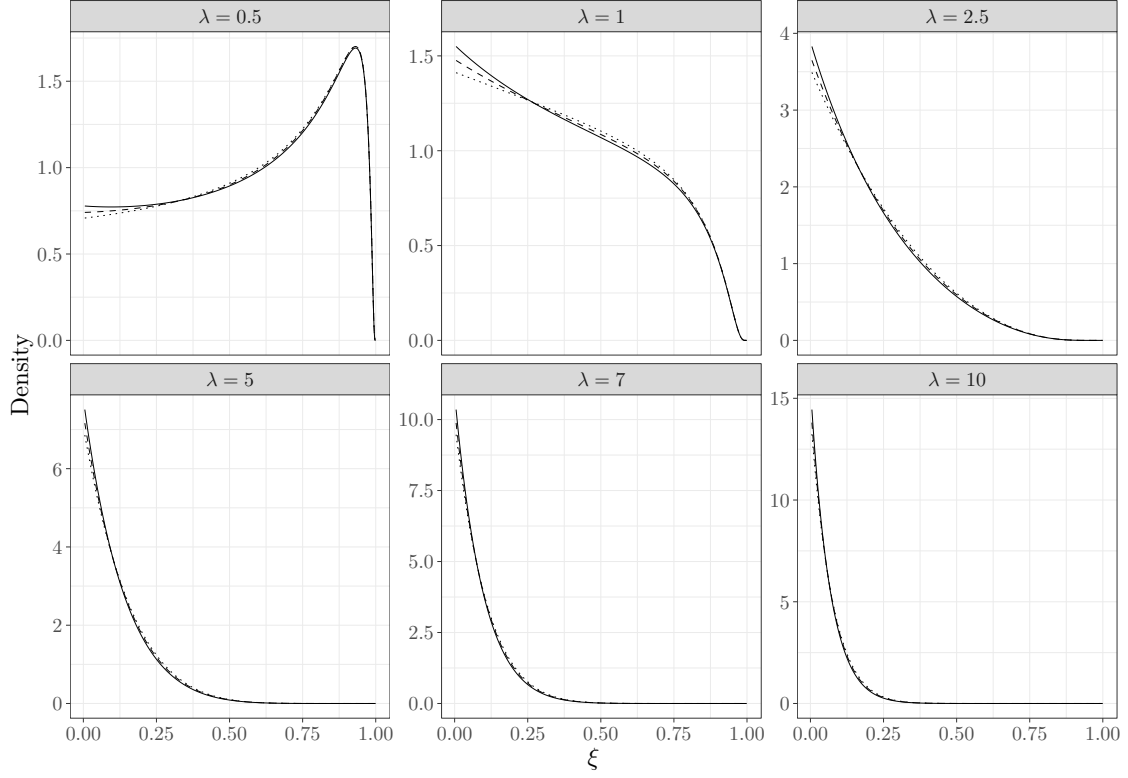


Figure A.1: PC priors with base models  $\xi = 0$  and different penalty parameters  $\lambda$  for the GEV (solid line), bGEV (dashed line) and GP distribution (dotted line).

The PC priors for the GEV, bGEV and generalised Pareto (GP) distributions are displayed in Figure A.1 for different values of the penalty parameter  $\lambda$ . For all the chosen values of  $\lambda$  the three distributions are so similar that their effect on a posterior distribution probably will be close to identical. The PC prior for the GP distribution exists in closed-form and is already implemented in R-INLA, while the other PC priors must be computed numerically and are not implemented in R-INLA. Consequently, we choose to use the PC prior of the GP distribution for modelling the tail parameter of the bGEV distribution.